Title: Impaired aldehyde detoxification caused by a common human polymorphism promotes anti-bacterial immunity

Authors: Scott Espich[1†], Sam Berry[2†], Amir Balakhmet[1], Xuling Chang[3,4,5], Nguyen T.T. Thuong[3,4], Rajkumar Dorajoo[4,8], Chiea-Chuen Khor[8,9], Chew-Kiat Heng[4,5], Jian-Min Yuan[10], Woon-Puay Koh[11,12], Douglas Fox[1], Andrea Anaya-Sanchez[13], Logan Tenney[14, 15],Christopher J. Chang[14,15, 16], Rishika Baral[1], Dmitri I. Kotov[1,16], Marietta Ravesloot-Chavez[1], Russell E. Vance[1,17], Sarah J. Dunstan[3], K. Heran Darwin[18,*], and Sarah A. Stanley[1,2,19,*]

[†]These authors contributed equally to this work

Affiliations:

1. Division of Immunology and Pathogenesis, Department of Molecular and Cell Biology, University of California, Berkeley, Berkeley, CA 94720
2. Department of Molecular and Cell Biology, University of California, Berkeley, Berkeley, CA 94720
3. Department of Infectious Diseases, University of Melbourne, at the Peter Doherty Institute for Infection and Immunity, Melbourne 3000, Australia Xu, SD
4. Department of Pediatrics, Yong Loo Lin School of Medicine, National University of Singapore and National University Health System, Singapore 119228, Singapore.
5. Khoo Teck Puat - National University Children's Medical Institute, National University Health System, Singapore, 119074, Singapore
6. Oxford University Clinical Research Unit, Ho Chi Minh City, Vietnam
7. Nuffield Department of Medicine, University of Oxford, Oxford, United Kingdom
8. Genome Institute of Singapore (GIS), Agency for Science, Technology and Research (A*STAR), 60 Biopolis Street, Genome, Singapore 138672, Republic of Singapore
9. Singapore Eye Research Institute, Singapore National Eye Centre, Singapore, 169856, Singapore
10. Division of Cancer Control and Population Sciences, UPMC Hillman Cancer Center, University of Pittsburgh, Pittsburgh, PA, 15232, USA. Department of Epidemiology, School of Public Health, University of Pittsburgh, Pittsburgh, PA, 15261, USA
11. Healthy Longevity Translational Research Programme, Yong Loo Lin School of Medicine, National University of Singapore, Singapore.
12. Institute for Human Development and Potential (IHDP), Agency for Science, Technology and Research (A*STAR), Singapore.
13. Graduate Group in Microbiology, University of California, Berkeley, Berkeley, CA 94720
14. Department of Chemistry, University of California, Berkeley, CA 94720
15. Department of Chemistry, Princeton University, Princeton, NJ 08544
16. Division of Molecular Therapeutics, Department of Molecular and Cell Biology, University of California, Berkeley, CA 94720
17. Howard Hughes Medical Institute, University of California, Berkeley
18. Department of Microbiology, New York University Grossman School of Medicine, New York, NY 10016.
19. Lead contact

*Correspondence: sastanley@berkeley.edu, heran.darwin@nyulangone.org

SUMMARY

The *ALDH2*2* (rs671) variant present in >500 million individuals reduces ALDH2 function, impairing aldehyde detoxification. While aldehyde accumulation in these individuals is associated with numerous negative health consequences, a previous study showed a cohort of *ALDH2*2* carriers are less likely to develop active pulmonary tuberculosis. Here, we present additional human data that support this finding and show ALDH2-deficiency in mice provides a fitness advantage during bacterial infections. We found aldehydes normally detoxified by ALDH2 killed the bacterial pathogens *Mycobacterium tuberculosis* and *Francisella tularensis.* Infected macrophages from *Aldh2*$^{-/-}$ mice had higher levels of formaldehyde and 4-hydroxynonenal, which enhanced their microbicidal capacity. *Aldh2*$^{-/-}$ mice were more resistant to infection with *Mycobacterium tuberculosis* and *Francisella tularensis* than parental mice and displayed elevated inflammatory cytokine and chemokine levels, accompanied by an increased accumulation of inflammatory monocytes and macrophages. These findings support a model in which host-derived aldehydes are robust innate immune effectors, limiting bacterial infection through both direct microbicidal activity and immune modulation. Collectively, this work may explain why the *ALDH2*2* allele was selected for in humans.

INTRODUCTION

Loss-of-function mutations in aldehyde dehydrogenase 2 (*ALDH2*) are highly prevalent, affecting up to 500 million individuals of East Asian descent[1]. The most common mutant allele, *ALDH2*2* (rs671), encodes a glutamate-to-lysine mutation at position 487, resulting in a dominant-negative form of the enzyme[2]. ALDH2 is notably required for converting acetaldehyde, a toxic intermediate of ethanol metabolism, into acetate, but its primary function is to detoxify metabolically produced aldehydes. Hetero- or homozygous carriers of *ALDH2*2* experience adverse physiological effects upon consumption of alcohol due to an accumulation of acetaldehyde[3]. Even in the absence of alcohol consumption, loss of ALDH2 function is associated with increased risk of cancer, heart disease, and neurological disorders[4,5]. Aldehydes can react with DNA, leading to mutations, and may disrupt cellular function by forming adducts with proteins, contributing to disease development[6–8]. Additionally, loss of ALDH2 activity has been associated with heightened inflammatory responses, which may further promote disease pathogenesis[9,10]. The selective pressure that has maintained *ALDH2*2* in the human population despite its detrimental effects on human health is unknown.

*ALDH2*2* was associated with a decreased risk of active tuberculosis (TB) in a cohort of Korean men. This correlation was hypothesized to be associated with decreased alcohol consumption[11]. While alcoholism is a significant risk factor for TB[12,13], we hypothesized that loss of ALDH2 function enhances resistance to bacterial infection independent of alcohol consumption. ALDH2 detoxifies many inflammation-induced aldehydes, including 4-hydroxynonenal (4HNE)[14–17], a lipid peroxidation end-product that is produced when macrophages and other innate immune cells generate reactive oxygen species in response to infection[16,18–20]. Additionally, ALDH2, along with alcohol dehydrogenase 5 (ADH5), metabolizes endogenous formaldehyde, which is produced by a range of cellular processes[21,22]. Formaldehyde production is also enhanced in the presence reactive oxygen species[23]. Together these studies suggest that loss of ALDH2 activity during infections could increase cellular aldehyde levels that would be toxic to invading

bacteria. Here, we demonstrate that loss of ALDH2 function enhances control of bacterial infection by promoting the microbicidal activity of macrophages and by accelerating inflammatory responses to infection.

RESULTS

ALDH2 rs671 is associated with lower pulmonary tuberculosis risk

Pulmonary tuberculosis (PTB) is the most common clinical manifestation of TB disease and leads to the principal mode of transmission amongst humans. To examine the relationship between the *ALDH2*2* mutation (rs671) and PTB, we performed a candidate gene analysis for cohorts in Vietnam and Singapore. Genotype data of rs671 was available from a collection of 1,598 microbiologically confirmed TB patients and 1,266 population controls from Vietnam (Figure 1A). In addition, the Singapore Chinese Health Study (SCHS) consists of 1,606 PTB cases and 23,969 population controls of Singaporean Chinese origin with available genotype data. A significant association between rs671 PTB was observed in both the Vietnamese cohort [OR (95% CI) = 0.855 (0.739, 0.990), P=0.036] and the SCHS [OR (95% CI) = 0.920 (0.850, 0.997), P=0.041] (Figure 1B), with the minor allele A associated with reduced PTB risk. After meta-analysis, the association was further strengthened ([OR (95% CI) = 0.905 (0.844, 0.971), P=0.005, $P_{heterogeneity}$=0.386]). We also assessed both dominant and recessive models of inheritance and found the dominant model returned associations of similar magnitude to the additive model [OR (95% CI) = 0.888 (0.813, 0.969), P=0.008, $P_{heterogeneity}$=0.429]. The modest effect sizes calculated, which were robustly replicated across two ethnic groups, are not unexpected, as the heritability of complex traits, such as infectious diseases, arises from the combined influence of numerous genetic variants, each contributing a modest effect size. These data, together with the previously published association study[11], support the hypothesis that the *ALDH2*2* rs671 mutation is associated with protection against PTB.

Aldh2 expression in macrophages is downregulated upon inflammatory stimulation

To determine whether ALDH2 is expressed in relevant cell types during infection, we examined *Aldh2* expression in the lungs of *M. tuberculosis* infected C57BL/6J ("WT") mice using single cell RNA sequencing (scRNAseq). *Aldh2* expression was observed in macrophage/monocyte populations, dendritic cells, neutrophils, basophils, B cells, pulmonary epithelial and endothelial cells, and fibroblasts (Figure S1A). Other immune cell types, such as T cells, did not express *Aldh2*. Macrophages serve both as the primary host cell for *M. tuberculosis* and a key effector cell in infection control, so we next investigated how infection alters *Aldh2* expression in bone marrow–derived macrophages (BMDMs) from WT mice. We infected BMDMs in the presence or absence of interferon-γ (IFNγ), a critical cytokine for macrophage activation and control of *M. tuberculosis* infection[24]. Consistent with the *in vivo* scRNA-seq data, ALDH2 protein was expressed in unstimulated BMDMs (Figure 1C). In contrast, IFNγ stimulation reduced *Aldh2* expression in both uninfected and *M. tuberculosis*-infected macrophages (Figure 1C), suggesting that IFNγ induces a transcriptional program that downregulates *Aldh2* expression during infection.

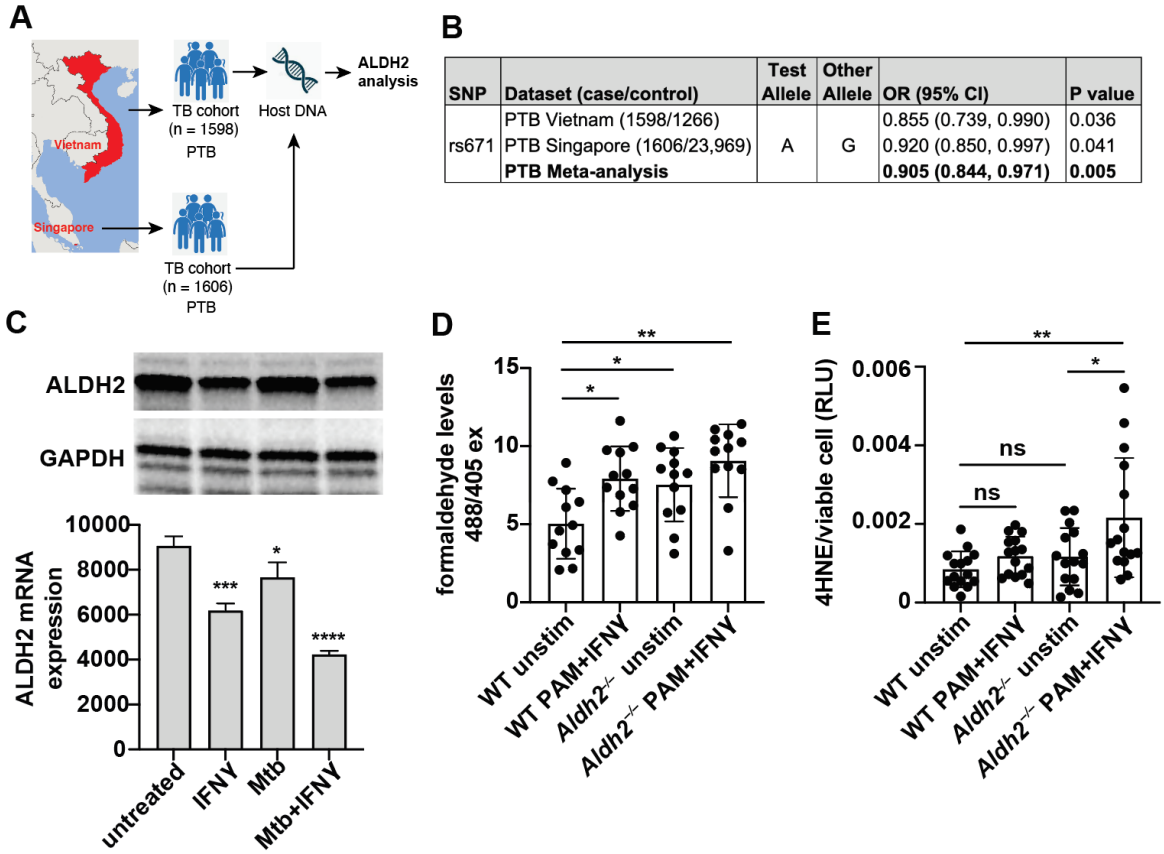

SNP	Dataset (case/control)	Test Allele	Other Allele	OR (95% CI)	P value
rs671	PTB Vietnam (1598/1266)	A	G	0.855 (0.739, 0.990)	0.036
	PTB Singapore (1606/23,969)			0.920 (0.850, 0.997)	0.041
	PTB Meta-analysis			**0.905 (0.844, 0.971)**	**0.005**

Figure 1. **ALDH2 expression is linked with human disease and immune activation**
(A, B) A candidate gene analysis of the ALDH2 rs671 mutation in pulmonary TB (PTB) patients in Vietnam and Singapore. (C) mRNA and protein for *Aldh2* expression *M. tuberculosis* infected C57BL/6J (WT) bone marrow-derived macrophages (BMDMs) stimulated with IFNγ and/or infected with *M. tuberculosis* H37Rv. (D) WT and *Aldh2*$^{-/-}$ BMDM mitochondrial-associated formaldehyde levels after 24 hours stimulation with IFNγ and PAM3CSK4 *in vitro.* (E) ELISA quantification of BMDM 4HNE after 24 hours stimulation with IFNγ and PAM3CSK4 *in vitro.* Experiments are representative of three independent experiments (C, D) or three independent experiments combined (E). (C, D) unpaired t-test, (E) Two-way ANOVA with Tukey's multiple comparisons test. *, $p < 0.05$, **, $p < 0.01$, ***, $p < 0.001$, ****, $p < 0.0001$.

Macrophages from *Aldh2*-deficient mice produce higher aldehyde levels

We next generated *Aldh2* mutant (*Aldh2*$^{-/-}$) mice using CRISPR-Cas9 (Figure S1B). The mutation (12 base pair deletion in exon 12 that encompasses the region where rs671 is found in humans) resulted in loss of ALDH2 as determined by immunoblotting (Figure S1C). We tested if immune activation could increase aldehyde production by wild-type (WT) macrophages and whether aldehyde production would be further enhanced by *Aldh2*-deficiency (Figure S1D). Using Mito-RFAP-2, a mitochondrial-targeted, ratio-metric dye that detects mitochondrial-localized formaldehyde with high sensitivity[25], we found that WT macrophages stimulated with IFNγ and PAM3CSK4, a TLR2 agonist, had increased formaldehyde 24 hours after stimulation (Figure 1D). This stimulation-induced enhancement of aldehyde production in macrophages inversely correlated with *Aldh2* expression (Figure 1C) and increased mitochondrial formaldehyde levels (Figure 1D). *Aldh2*$^{-/-}$ macrophages produced significantly more

formaldehyde than the WT cells in the absence of immune stimulation (Figure 1D). A significant difference was not observed between stimulated and unstimulated *Aldh2*$^{-/-}$ macrophages, suggesting that formaldehyde levels in *Aldh2*$^{-/-}$ macrophages could not be further increased by external stimulation.

We next measured 4HNE-protein adducts by ELISA. Although we observed a trend towards increased 4HNE production in response to stimulation with PAM3CSK4 and IFNγ in WT macrophages, it was not significantly different between stimulated and resting macrophages (Figure 1E). However, stimulated *Aldh2*$^{-/-}$ macrophages produced higher levels of 4HNE than stimulated WT or unstimulated *Aldh2*$^{-/-}$ macrophages (Figure 1E).

Aldehydes detoxified by ALDH2 kill *M. tuberculosis*

Based on the role of ALDH2 in detoxifying inflammation-associated aldehydes, we tested the susceptibility of *M. tuberculosis* to 4HNE and formaldehyde in axenic culture. 4HNE can reach millimolar concentrations in inflamed tissues[8,15,26], and formaldehyde has been found at up to 400 μM in blood and tissues[27–29]. Using a standard half-maximal inhibitory concentration (IC_{50}) protocol, we found the *in vitro* IC_{50} values range between 40-150 μM for formaldehyde while 4HNE had an IC_{50} of 40 μM. *M. tuberculosis* was sensitive to 4HNE, with 10-fold killing observed at 50 μM after six days of exposure and greater than three orders of magnitude of toxicity at 200 μM (Figure 2A) relative to controls. Similarly, we found that formaldehyde was toxic to *M. tuberculosis* at 100 μM (Figure 2B). Thus, *M. tuberculosis* is susceptible to physiologically relevant levels of aldehyde in broth culture.

Mice lacking *Aldh2* exhibit reduced susceptibility to *M. tuberculosis* infection

We next tested whether ALDH2 deficiency enhances control of *M. tuberculosis* by infected macrophages. WT and *Aldh2*$^{-/-}$ macrophages were infected with *M. tuberculosis* at a multiplicity of infection of one bacillus per macrophage (MOI = 1), and bacterial replication was monitored over four days. *M. tuberculosis* replication was identical in WT and *Aldh2*$^{-/-}$ macrophages (Figure 2C). We observed the expected restriction of *M. tuberculosis* growth after IFNγ activation, but we did not observe significant differences between the WT and *Aldh2*$^{-/-}$ BMDMs (Figure 2C). Given that *in vitro* conditions neither recapitulate the extent of inflammation nor the complete pathogenesis observed *in vivo*, we infected *Aldh2*$^{-/-}$ mice to assess the role of ALDH2 in a biologically relevant model of *M. tuberculosis.* We infected mice via the aerosol route with a low-to-medium dose (~25 colony forming units, CFU) of *M. tuberculosis* and harvested their lungs for CFU enumeration at various time points. At 14 days post infection (dpi), we observed no difference in the ability of *Aldh2*$^{-/-}$ mice to control pulmonary infection when compared with littermate controls (Figure 2D); however, at 28 dpi, we observed a significant difference between *Aldh2*$^{-/-}$ mice and WT mice, wherein *Aldh2*$^{-/-}$ mice had lower bacterial burdens (Figure 2D). The adaptive immune response is typically observed after 14 dpi in mice, where increased IFNγ signaling results from T cell migration to the site of infection. This result suggests that sustained T cell-mediated IFNγ signaling may contribute to the improved control observed by the *Aldh2*$^{-/-}$ mice at 28 dpi by increasing local aldehyde production. WT mice are relatively resistant to infection with *M. tuberculosis*[30,31].

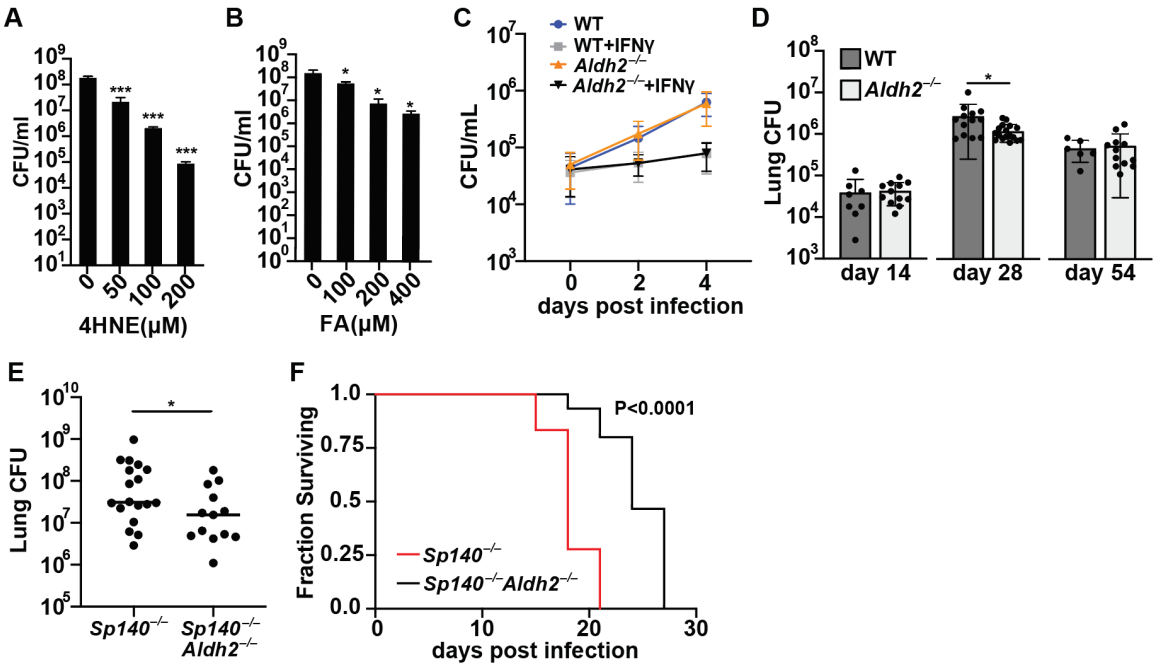

Figure 2. *Aldh2*-deficient mice exhibit enhanced control of *M. tuberculosis* infection
M. tuberculosis H37Rv killing after six days treatment with physiological levels of (A) 4-hydroxynonenal (4HNE) or (B) Formaldehyde (FA). (C) CFU enumeration of WT and *Aldh2*$^{-/-}$ BMDMs infected with *M. tuberculosis* LuxErd +/- IFNγ at an MOI= 1. (D) Lung CFU enumeration of aerosol-infected *Aldh2*$^{-/-}$ and WT mice with ≈ 25 CFU *M. tuberculosis* H37Rv at indicated timepoints. (E) Lung CFU enumeration of aerosol-infected *Sp140*$^{-/-}$ and *Sp140*$^{-/-}$*Aldh2*$^{-/-}$ mice with ≈ 25 CFU *M. tuberculosis* Erdman 28 dpi. (F) Survival curve of *Sp140*$^{-/-}$ and *Sp140*$^{-/-}$*Aldh2*$^{-/-}$ mice infected with a high dose of *M. tuberculosis* Erdman (300 CFU). (A), (B) *p<0.05 by unpaired t-test. (D), (E) p<0.05 by Mann-Whitney. (F) p<0.0001 by Mantel-Cox log rank test. Experiments are representative of a minimum of three (A), (B), (C), (F) or three experiments combined (D), (E).

We hypothesized that the protective effect of ALDH2 could be more robust in a susceptible mouse background in which a loss of bacterial control correlates with destructive inflammatory responses in the lung, as well as in a setting of increased aldehyde load. To test this hypothesis, we generated *Aldh*$^{-/-}$ mice on the background of *Sp140* deficiency. *Sp140*$^{-/-}$ mice have type I IFN-driven susceptibility to disease and severe bacterial burden during *M. tuberculosis* infection[32]. We infected *Aldh2*$^{-/-}$ *Sp140*$^{-/-}$ and parental *Sp140*$^{-/-}$ mice with *M. tuberculosis*. Both genotypes had increased lung CFU relative to *Aldh2*$^{-/-}$ and WT mice due to the known susceptibility of the *Sp140*$^{-/-}$ background (Figure 2E). As with WT mice, we observed significantly fewer CFU in the *Aldh2*$^{-/-}$*Sp140*$^{-/-}$ mice when compared to parental *Sp140*$^{-/-}$ animals at 28 dpi (Figure 2E). To determine if *Aldh2* deficiency promotes survival during infection in this context, we infected *Aldh2*$^{-/-}$*Sp140*$^{-/-}$ mice with a high dose of *M. tuberculosis.* *Aldh2*$^{-/-}$*Sp140*$^{-/-}$ mice lived significantly longer that the *Sp140*$^{-/-}$controls (Figure 2F). Thus, even in the presence of a host-detrimental inflammatory type I IFN response, disruption of *Aldh2* had a protective effect against *M. tuberculosis* infection.

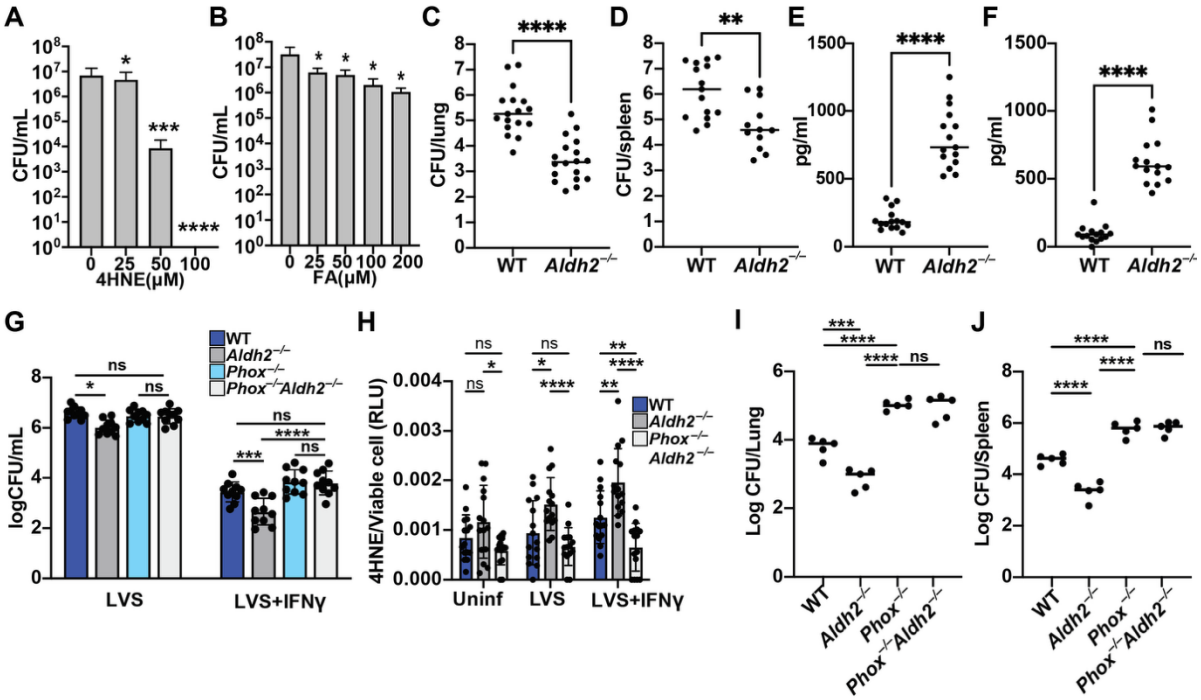

Figure 3. *F. tularensis* LVS growth is attenuated in *Aldh2*$^{-/-}$ mice and macrophages
F. tularensis LVS (FtLVS) killing after two hours of treatment with physiological levels of (A) 4HNE or (B) formaldehyde. CFU enumeration of WT and *Aldh2*$^{-/-}$ lungs (C) or spleens (D) infected with 10^5 FtLVS i.d., five dpi. 4HNE quantification in WT and *Aldh2*$^{-/-}$ lungs (E) or spleens (F) infected with 10^5 FtLVS i.d., 3 dpi. (G) CFU enumeration of WT and *Aldh2*$^{-/-}$ BMDMs infected with FtLVS +/- IFNγ at an MOI= 1. (H) 4HNE quantification in untreated or FtLVS infected BMDMs +/- IFNγ. FtLVS CFU enumeration in (I) lungs or (J) spleens of WT, *Aldh2*$^{-/-}$, *p47phox*$^{-/-}$ and *Aldh2*$^{-/-}$ *p47phox*$^{-/-}$ mice infected with 10^3 FtLVS i.d., 5 dpi. *p<0.05, **p<0.01, ***p<0.001, ****p<0.0001. (A-D) unpaired t-test. (E, F) Mann-Whitney. (G, H) 2way ANOVA with Tukey's multiple comparisons test. (I-J) one-way ANOVA with Dunnett's multiple comparisons test. Experiments are representative of a minimum of three (A), (B), (I), (J) or three experiments combined (C-H).

Aldh2 deficiency enhances control of *Francisella* infection

Previous work demonstrated the susceptibility of *Francisella* species to 4HNE and other metabolic aldehydes[33,34]. We observed that the *Francisella tularensis* Live Vaccine Strain (FtLVS) was highly susceptible to 4HNE and formaldehyde, showing nearly three orders of magnitude of killing with 50 μM 4HNE, and ~1 log killing with 25 μM formaldehyde (Figures 3A and 3B). To test whether *Aldh2*$^{-/-}$ mice are resistant to infection with FtLVS, we infected mice with FtLVS intradermally (i.d.) and measured CFU in lungs and spleens five days later. We found that in both organs, *Aldh2*$^{-/-}$ mice had significantly lower bacterial burdens than parental mice (Figures 3C and 3D). We also observed elevated levels of 4HNE concentrations in tissues of infected *Aldh2*$^{-/-}$ mice (Figures 3E and 3F). Because macrophages are a primary replicative niche for FtLVS[35], we next reasoned that enhanced control of infection in *Aldh2*$^{-/-}$ mice could be associated with enhanced macrophage microbicidal activity. To test this hypothesis, we infected BMDMs from WT and *Aldh2*$^{-/-}$ mice *in vitro* and found that *Aldh2*$^{-/-}$ macrophages were indeed more microbicidal than WT macrophages, an effect that was enhanced by IFNγ stimulation

250 (Figure 3G). CFU was equivalent across genotypes on day 0, and no differences in macrophage
251 viability were observed at any timepoint (Figures S3J and S3K).
252
253 To further correlate the microbicidal activity of *Aldh2*$^{-/-}$ macrophages with elevated aldehyde
254 levels, we sought to abolish infection-associated aldehyde production in *Aldh2*$^{-/-}$ macrophages
255 and mice. Lipid peroxidation reactions downstream of NADPH oxidase are the primary source
256 of 4HNE in activated macrophages[36]. Consistent with this observation, we found that
257 macrophages lacking both *Aldh2* and *p47phox* (*phox*$^{-/-}$), a subunit of NADPH oxidase, had WT
258 4HNE levels after infection with FtLVS (Figure 3H). Consistent with the lowered aldehyde levels,
259 loss of *p47phox* also abolished the enhanced control of infection observed in *Aldh2*$^{-/-}$
260 macrophages (Figure 3G). Deletion of *p47phox* also reversed *Aldh2* dependent control of FtLVS
261 infection in vivo (Figures 3I and 3J). We were unable to consistently detect formaldehyde in
262 FtLVS infected macrophages.
263
264 ***Aldh2*$^{-/-}$ mice have enhanced innate responses to FtLVS infection**
265 To test whether differences in inflammatory responses contribute to enhanced FtLVS control in
266 *Aldh2*$^{-/-}$ mice, we analyzed pulmonary and splenic immune responses three dpi., a timepoint
267 preceding significant differences in bacterial burden (Figures 4A and 4B). We found that
268 *Aldh2*$^{-/-}$ mice showed a selective increase in recruitment of inflammatory monocytes (iMOS) and
269 inducible nitric oxide synthase (iNOS)-expressing macrophages relative to WT controls.
270 Frequencies of neutrophils and other cell types remained comparable between genotypes
271 (Figures 4C-H and S4). Further, we found that Chemokine (C-C motif) ligand 2 (CCL2) levels
272 were elevated in both the lungs and spleens of *Aldh2*$^{-/-}$ mice, explaining the increased
273 recruitment of monocytes and macrophages (Figures 4I and 4J). In addition to CCL2, we found
274 that numerous inflammatory cytokines were elevated in *Aldh2*$^{-/-}$ spleens and lungs (Figures
275 S3A-I). Although iNOS^{+} macrophages were enriched in the spleen and lungs of *Aldh2*$^{-/-}$ mice,
276 protection was maintained in the absence of iNOS, indicating that aldehyde-mediated control is
277 independent of NO production under these conditions (Figures 4K and 4L).

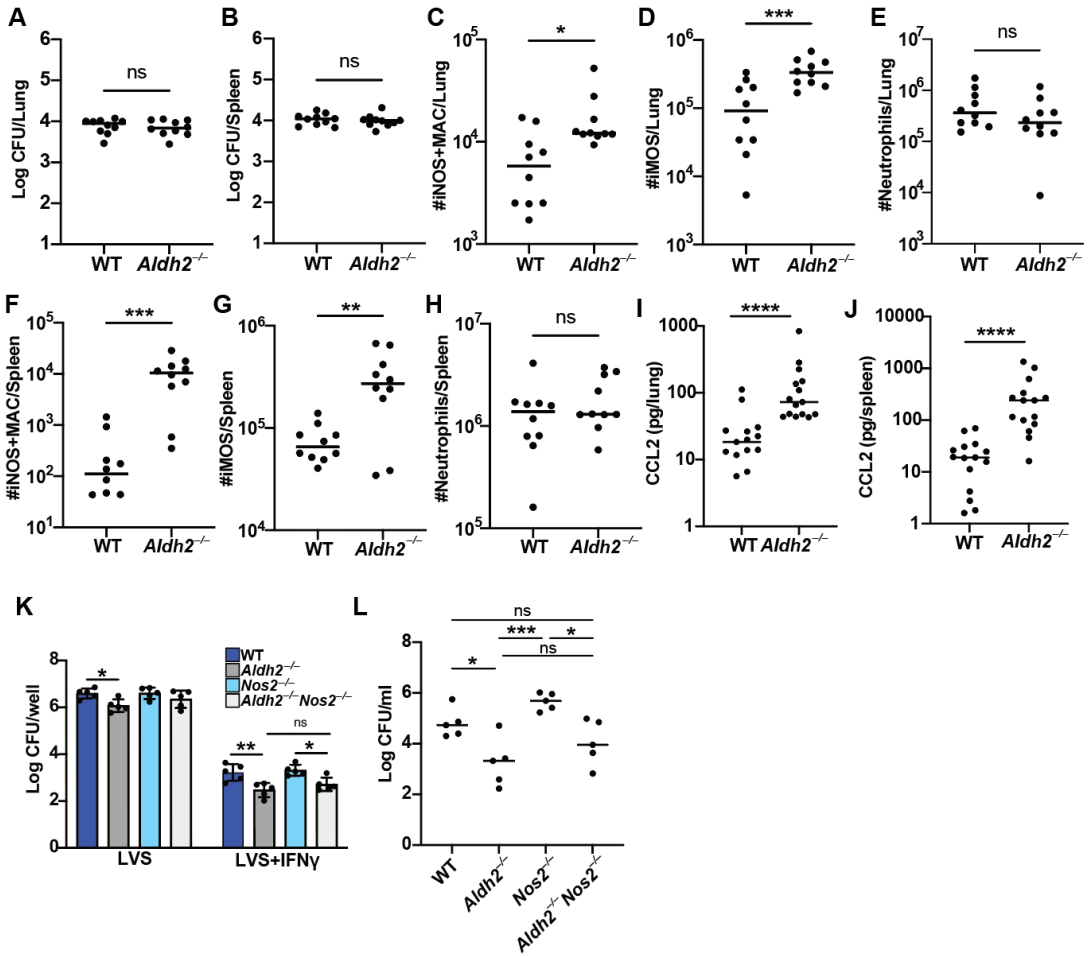

Figure 4. *Aldh2*$^{-/-}$ mice exhibit heightened innate immune activation following *F. tularensis* LVS infection

CFU enumeration of lung (A) and spleen (B) in WT and *Aldh2*$^{-/-}$ mice infected with 10^5 FtLVS i.d., 3 dpi. Frequencies of iNOS$^+$ macrophages (C) inflammatory monocytes (D) and neutrophils (E) in the lungs of WT and *Aldh2*$^{-/-}$ mice infected with 10^5 FtLVS i.d, 3 dpi. Frequencies of iNOS$^+$ macrophages (F) inflammatory monocytes (G) and neutrophils (H) in the spleens of WT and *Aldh2*$^{-/-}$ mice infected with 10^5 FtLVS i.d., 3 dpi. CCL2 quantification in the lungs (I) and spleens (J) of WT and *Aldh2*$^{-/-}$ mice infected with 10^5 FtLVS i.d., 3 dpi. (K) CFU enumeration in WT, *Aldh2*$^{-/-}$, *Nos2*$^{-/-}$, and *Nos2*$^{-/-}$*Aldh2*$^{-/-}$ infected with FtLVS MOI=1, +/- IFNγ, 2 dpi. L) CFU enumeration in WT, *Aldh2*$^{-/-}$,*Nos2*$^{-/-}$, and *Nos2*$^{-/-}$*Aldh2*$^{-/-}$ mice infected with 10^3 FtLVS, 5 dpi. *p<0.05, **p<0.01, ***p<0.001, ****p<0.0001. (A), (B): unpaired t-test. (C-J): Mann-Whitney test. (K): 2way ANOVA with Tukey's multiple comparisons test. (L): one-way ANOVA with Dunnett's multiple comparisons test. Experiments are representative of a minimum of three (A-J), (K), (L) or three experiments combined (I), (J).

DISCUSSION

Throughout human history, pathogens have acted as powerful selective forces, shaping the genetic architecture of modern populations. Classic examples, such as the persistence of the sickle cell allele in malaria endemic regions, illustrate how genetic variants that confer resistance to pathogens can be maintained despite associated fitness costs. In this context, our findings suggest that the widespread ALDH2*2 allele, though traditionally associated with

alcohol intolerance, may represent an evolutionary adaptation to bacterial infection[37]. We show that ALDH2 deficiency confers enhanced protection against *Mycobacterium tuberculosis* and *Francisella tularensis* LVS, both in humans (for Mtb) and in mouse models (both pathogens). Mechanistically, *Aldh2*$^{-/-}$ mice and macrophages have elevated levels of bactericidal 4HNE and formaldehyde, enhanced innate immune activation, and increased bacterial killing. Taken together, our results support a model in which loss of ALDH2 function amplifies aldehyde-mediated antimicrobial activity, potentially explaining the positive selection of *ALDH2*2* in pathogen-exposed populations. This may represent a previously unrecognized instance of balancing selection, in which antagonistic pleiotropy maintains *ALDH2*2*, despite its deleterious effects, by enhancing protection against infection.

The *ALDH2*2* allele is predicted to have evolved about 3,000 years ago[38] and is predominantly found in individuals of east Asian descent; interestingly, the emergence of *M. tuberculosis* lineage 2 (also known as the W/Beijing lineage) occurred between 2,000 – 7,000 years ago[38,39], and this lineage is more prevalent in East Asia. In congruence with previous data[11], we found that individuals harboring the *ALDH2*2* allele have a reduced risk of developing PTB, suggesting that there may have been evolutionary pressure selecting for this allele in environments where TB transmission was high. Lineage 2 strains exhibit increased transmissibility, hypervirulence, and a higher mutation rate[40–43], all of which may facilitate survival under host-imposed antimicrobial pressures—including aldehyde stress. Further research is needed to explore if there is an evolutionary interplay between *ALDH2*2* and lineage 2 strains.

Although *Aldh2*$^{-/-}$ mice showed early protection against *M. tuberculosis,* we did not observe differences in bacterial burden at later timepoints. One explanation is that in the relatively resistant B6 background, infection becomes persistent and controlled by 28-56 dpi, with limited bacterial replication and dampened inflammation, conditions under which aldehyde-mediated killing may be less effective. In contrast, *Aldh2* deficiency confers an advantage in *Sp140*$^{-/-}$ mice, even when infection is acute and poorly controlled. Consistent with this result, we observed robust protection in *Aldh2*$^{-/-}$ mice challenged with FtLVS, a model of acute, rapidly progressive infection. Importantly, our finding that individuals carrying the *ALDH2*2* allele have reduced risk of PTB suggests that even modest enhancements in early host control may confer meaningful protection in natural infection settings.

ALDH2 deficiency has been associated with heightened inflammation in both clinical and experimental settings[10,44]. The accumulation of reactive aldehydes can act as an endogenous danger signal by modifying host proteins and activating stress and immune signaling pathways[45]. Our findings extend this connection to the context of infection. Notably, protection in *Aldh2*$^{-/-}$ mice and macrophages was dependent on NADPH oxidase, which drives reactive oxygen species production within the phagosome following bacterial phagocytosis. This result suggests that aldehydes produced via phagosomal lipid peroxidation reactions are required for protection observed in *Aldh2*$^{-/-}$ mice. Further, flow cytometry analysis revealed that *Aldh2*$^{-/-}$ mice infected with FtLVS exhibited increased recruitment of inflammatory monocytes and macrophages to infected tissues, which was accompanied by elevated levels CCL2 and IFNγ, a

343 potent inflammatory macrophage activator required to protect against FtLVS infection. These
344 data suggest that NADPH oxidase-driven aldehyde accumulation not only contributes to direct
345 bacterial killing but may also amplify innate immune activation that promotes pathogen
346 clearance. This idea is consistent with previous studies that show that *ALDH2* deficiency is
347 associated with increased frequencies of inflammatory macrophages[46].
348
349 FtLVS evades early innate immune recognition, a strategy critical for its pathogenesis[47].
350 Aldehyde-induced early inflammation may disrupt this evasion, restricting bacterial replication
351 and partially attenuating infection. Supporting this hypothesis, pharmacological inhibition of
352 ALDH2 increases macrophage resistance to FtLVS infection *in vitro,* suggesting that aldehyde
353 accumulation alone may be sufficient to enhance antibacterial immunity[48]. While our study
354 focused on 4HNE and formaldehyde, ALDH2 detoxifies a broad spectrum of endogenous
355 aldehydes, including malondialdehyde and acrolein, which may also accumulate in *Aldh2*$^{-/-}$
356 mice and contribute to host protection. Future work will define the full repertoire of
357 immunomodulatory and antimicrobial aldehydes regulated by ALDH2, and how their cumulative
358 effects shape the immune response to infection.
359
360 Collectively, our findings highlight the dual role of aldehydes as both cytotoxic metabolites and
361 immune effectors[37]. More broadly, this work underscores the importance of metabolic regulation
362 in innate immunity and suggests that host-derived aldehydes represent a novel class of
363 endogenous antimicrobial factors weaponized by host cells to combat pathogens. Elucidating
364 how these reactive metabolites function in different infection models and inflammatory contexts
365 may open new avenues for host-directed therapeutic strategies.
366

RESOURCE AVAILABILITY

Lead contact

Further information and requests for resources and reagents should be directed to, and will be fulfilled by, the lead contact, Sarah A. Stanley (sastanley@berkeley.edu).

Materials availability

All reagents generated or used in this study are available on request from the lead contact with a completed materials transfer agreement.

Data and code availability

All data reported in this paper will be shared by the lead contact upon request. Any additional information required to reanalyze the data reported in this work paper is available from the lead contact upon request.

References:

1. Chen, C.-H., Kraemer, B.R., and Mochly-Rosen, D. (2022). ALDH2 variance in disease and populations. Dis. Model. Mech. *15*. https://doi.org/10.1242/dmm.049601.

2. Impraim, C., Wang, G., and Yoshida, A. (1982). Structural mutation in a major human aldehyde dehydrogenase gene results in loss of enzyme activity. Am. J. Hum. Genet. *34*, 837–841.

3. Harada, S., Agarwal, D.P., and Goedde, H.W. (1981). Aldehyde dehydrogenase deficiency as cause of facial flushing reaction to alcohol in Japanese. Lancet *2*, 982.

4. Gross, E.R., Zambelli, V.O., Small, B.A., Ferreira, J.C.B., Chen, C.-H., and Mochly-Rosen, D. (2015). A personalized medicine approach for Asian Americans with the aldehyde dehydrogenase 2*2 variant. Annu. Rev. Pharmacol. Toxicol. *55*, 107–127.

5. Chen, C.-H., Ferreira, J.C.B., Gross, E.R., and Mochly-Rosen, D. (2014). Targeting aldehyde dehydrogenase 2: new therapeutic opportunities. Physiol. Rev. *94*, 1–34.

6. Vijayraghavan, S., and Saini, N. (2023). Aldehyde-associated Mutagenesis—Current state of knowledge. Chem. Res. Toxicol. *36*, 983–1001.

7. Oka, Y., Hamada, M., Nakazawa, Y., Muramatsu, H., Okuno, Y., Higasa, K., Shimada, M., Takeshima, H., Hanada, K., Hirano, T., et al. (2020). Digenic mutations in ALDH2 and ADH5 impair formaldehyde clearance and cause a multisystem disorder, AMeD syndrome. Sci. Adv. *6*, eabd7197.

8. Dalleau, S., Baradat, M., Guéraud, F., and Huc, L. (2013). Cell death and diseases related to oxidative stress: 4-hydroxynonenal (HNE) in the balance. Cell Death Differ. *20*, 1615–1630.

9. Ma, H., Lou, K., Shu, Q., Song, X., and Xu, H. (2024). Aldehyde dehydrogenase 2 deficiency reinforces formaldehyde-potentiated pro-inflammatory responses and glycolysis in macrophages. J. Biochem. Mol. Toxicol. *38*, e23518.

408 10. Pan, C., Xing, J.-H., Zhang, C., Zhang, Y.-M., Zhang, L.-T., Wei, S.-J., Zhang, M.-X., Wang,
409 X.-P., Yuan, Q.-H., Xue, L., et al. (2016). Aldehyde dehydrogenase 2 inhibits inflammatory
410 response and regulates atherosclerotic plaque. Oncotarget *7*, 35562–35576.

411 11. Park, S.K., Park, C.-S., Lee, H.-S., Park, K.S., Park, B.L., Cheong, H.S., and Shin, H.D.
412 (2014). Functional polymorphism in aldehyde dehydrogenase-2 gene associated with risk
413 of tuberculosis. BMC Med. Genet. *15*, 40.

414 12. Rehm, J., Samokhvalov, A.V., Neuman, M.G., Room, R., Parry, C., Lönnroth, K., Patra, J.,
415 Poznyak, V., and Popova, S. (2009). The association between alcohol use, alcohol use
416 disorders and tuberculosis (TB). A systematic review. BMC Public Health *9*, 450.

417 13. Imtiaz, S., Shield, K.D., Roerecke, M., Samokhvalov, A.V., Lönnroth, K., and Rehm, J.
418 (2017). Alcohol consumption as a risk factor for tuberculosis: meta-analyses and burden of
419 disease. Eur. Respir. J. *50*. https://doi.org/10.1183/13993003.00216-2017.

420 14. Barrera, G., Pizzimenti, S., Ciamporcero, E.S., Daga, M., Ullio, C., Arcaro, A., Cetrangolo,
421 G.P., Ferretti, C., Dianzani, C., Lepore, A., et al. (2015). Role of 4-hydroxynonenal-protein
422 adducts in human diseases. Antioxid. Redox Signal. *22*, 1681–1702.

423 15. Shoeb, M., Ansari, N.H., Srivastava, S.K., and Ramana, K.V. (2014). 4-Hydroxynonenal in
424 the pathogenesis and progression of human diseases. Curr. Med. Chem. *21*, 230–237.

425 16. Schaur, R.J., Siems, W., Bresgen, N., and Eckl, P.M. (2015). 4-Hydroxy-nonenal-A
426 Bioactive Lipid Peroxidation Product. Biomolecules *5*, 2247–2337.

427 17. Anderson, E.J., Katunga, L.A., and Willis, M.S. (2012). Mitochondria as a source and target
428 of lipid peroxidation products in healthy and diseased heart. Clin. Exp. Pharmacol. Physiol.
429 *39*, 179–193.

430 18. Breitzig, M., Bhimineni, C., Lockey, R., and Kolliputi, N. (2016). 4-Hydroxy-2-nonenal: a
431 critical target in oxidative stress? Am. J. Physiol. Cell Physiol. *311*, C537–C543.

432 19. Yoval-Sánchez, B., and Rodríguez-Zavala, J.S. (2012). Differences in susceptibility to
433 inactivation of human aldehyde dehydrogenases by lipid peroxidation byproducts. Chem.
434 Res. Toxicol. *25*, 722–729.

435 20. Ayala, A., Muñoz, M.F., and Argüelles, S. (2014). Lipid peroxidation: production,
436 metabolism, and signaling mechanisms of malondialdehyde and 4-hydroxy-2-nonenal.
437 Oxid. Med. Cell. Longev. *2014*, 360438.

438 21. Dingler, F.A., Wang, M., Mu, A., Millington, C.L., Oberbeck, N., Watcham, S., Pontel, L.B.,
439 Kamimae-Lanning, A.N., Langevin, F., Nadler, C., et al. (2020). Two Aldehyde Clearance
440 Systems Are Essential to Prevent Lethal Formaldehyde Accumulation in Mice and Humans.
441 Mol. Cell *80*, 996-1012.e9.

442 22. Nakamura, J., Holley, D.W., Kawamoto, T., and Bultman, S.J. (2020). The failure of two
443 major formaldehyde catabolism enzymes (ADH5 and ALDH2) leads to partial synthetic
444 lethality in C57BL/6 mice. Genes Environ *42*, 21.

445 23. Morellato, A.E., Umansky, C., and Pontel, L.B. (2021). The toxic side of one-carbon
446 metabolism and epigenetics. Redox Biol. *40*, 101850.

24. Flynn, J.L., Chan, J., Triebold, K.J., Dalton, D.K., Stewart, T.A., and Bloom, B.R. (1993). An essential role for interferon gamma in resistance to Mycobacterium tuberculosis infection. J. Exp. Med. *178*, 2249–2254.

25. Tenney, L., Pham, V.N., Brewer, T.F., and Chang, C.J. (2024). A mitochondrial-targeted activity-based sensing probe for ratiometric imaging of formaldehyde reveals key regulators of the mitochondrial one-carbon pool. Chem. Sci. *15*, 8080–8088.

26. Mihalas, B.P., De Iuliis, G.N., Redgrove, K.A., McLaughlin, E.A., and Nixon, B. (2017). The lipid peroxidation product 4-hydroxynonenal contributes to oxidative stress-mediated deterioration of the ageing oocyte. Sci. Rep. *7*, 6247.

27. Burgos-Barragan, G., Wit, N., Meiser, J., Dingler, F.A., Pietzke, M., Mulderrig, L., Pontel, L.B., Rosado, I.V., Brewer, T.F., Cordell, R.L., et al. (2017). Mammals divert endogenous genotoxic formaldehyde into one-carbon metabolism. Nature *548*, 549–554.

28. Heck, H.D., Casanova-Schmitz, M., Dodd, P.B., Schachter, E.N., Witek, T.J., and Tosun, T. (1985). Formaldehyde (CH2O) concentrations in the blood of humans and Fischer-344 rats exposed to CH2O under controlled conditions. Am. Ind. Hyg. Assoc. J. *46*, 1–3.

29. Luo, W., Li, H., Zhang, Y., and Ang, C.Y. (2001). Determination of formaldehyde in blood plasma by high-performance liquid chromatography with fluorescence detection. J. Chromatogr. B Biomed. Sci. Appl. *753*, 253–257.

30. Cooper, A.M. (2014). Mouse model of tuberculosis. Cold Spring Harb. Perspect. Med. *5*, a018556.

31. Medina, E., and North, R.J. (1998). Resistance ranking of some common inbred mouse strains to Mycobacterium tuberculosis and relationship to major histocompatibility complex haplotype and Nramp1 genotype. Immunology *93*, 270–274.

32. Ji, D.X., Witt, K.C., Kotov, D.I., Margolis, S.R., Louie, A., Chevée, V., Chen, K.J., Gaidt, M.M., Dhaliwal, H.S., Lee, A.Y., et al. (2021). Role of the transcriptional regulator SP140 in resistance to bacterial infections via repression of type I interferons. Elife *10*. https://doi.org/10.7554/eLife.67290.

33. Tabakh, H., McFarland, A.P., Thomason, M.K., Pollock, A.J., Glover, R.C., Zaver, S.A., and Woodward, J.J. (2021). 4-Hydroxy-2-nonenal antimicrobial toxicity is neutralized by an intracellular pathogen. Elife *10*. https://doi.org/10.7554/eLife.59295.

34. Anaya-Sanchez, A., Berry, S.B., Espich, S., Zilinskas, A., Tran, P.M., Agudelo, C., Samani, H., Darwin, K.H., Portnoy, D.A., and Stanley, S.A. (2025). Methylglyoxal is an antibacterial effector produced by macrophages during infection. Cell Host Microbe. https://doi.org/10.1016/j.chom.2025.05.026.

35. Elkins, K.L., Cowley, S.C., and Bosio, C.M. (2007). Innate and adaptive immunity to Francisella. Ann. N. Y. Acad. Sci. *1105*, 284–324.

36. Ioannidis, M., Tjepkema, J., Uitbeijerse, M.R.P., and van den Bogaart, G. (2025). Immunomodulatory effects of 4-hydroxynonenal. Redox Biol. *85*, 103719.

485 37. Darwin, K.H., and Stanley, S.A. (2022). The aldehyde hypothesis: metabolic intermediates
486 as antimicrobial effectors. Open Biol. *12*, 220010.

487 38. Liu, Q., Ma, A., Wei, L., Pang, Y., Wu, B., Luo, T., Zhou, Y., Zheng, H.-X., Jiang, Q., Gan,
488 M., et al. (2018). China's tuberculosis epidemic stems from historical expansion of four
489 strains of Mycobacterium tuberculosis. Nat Ecol Evol *2*, 1982–1992.

490 39. Merker, M., Blin, C., Mona, S., Duforet-Frebourg, N., Lecher, S., Willery, E., Blum, M.G.B.,
491 Rüsch-Gerdes, S., Mokrousov, I., Aleksic, E., et al. (2015). Evolutionary history and global
492 spread of the Mycobacterium tuberculosis Beijing lineage. Nat. Genet. *47*, 242–249.

493 40. Hanekom, M., Gey van Pittius, N.C., McEvoy, C., Victor, T.C., Van Helden, P.D., and
494 Warren, R.M. (2011). Mycobacterium tuberculosis Beijing genotype: a template for
495 success. Tuberculosis *91*, 510–523.

496 41. Parwati, I., van Crevel, R., and van Soolingen, D. (2010). Possible underlying mechanisms
497 for successful emergence of the Mycobacterium tuberculosis Beijing genotype strains.
498 Lancet Infect. Dis. *10*, 103–111.

499 42. Holt, K.E., McAdam, P., Thai, P.V.K., Thuong, N.T.T., Ha, D.T.M., Lan, N.N., Lan, N.H.,
500 Nhu, N.T.Q., Hai, H.T., Ha, V.T.N., et al. (2018). Frequent transmission of the
501 Mycobacterium tuberculosis Beijing lineage and positive selection for the EsxW Beijing
502 variant in Vietnam. Nat. Genet. *50*, 849–856.

503 43. Ford, C.B., Shah, R.R., Maeda, M.K., Gagneux, S., Murray, M.B., Cohen, T., Johnston,
504 J.C., Gardy, J., Lipsitch, M., and Fortune, S.M. (2013). Mycobacterium tuberculosis
505 mutation rate estimates from different lineages predict substantial differences in the
506 emergence of drug-resistant tuberculosis. Nat. Genet. *45*, 784–790.

507 44. Joshi, A.U., Van Wassenhove, L.D., Logas, K.R., Minhas, P.S., Andreasson, K.I.,
508 Weinberg, K.I., Chen, C.-H., and Mochly-Rosen, D. (2019). Aldehyde dehydrogenase 2
509 activity and aldehydic load contribute to neuroinflammation and Alzheimer's disease related
510 pathology. Acta Neuropathol. Commun. *7*, 190.

511 45. Binder, C.J., Papac-Milicevic, N., and Witztum, J.L. (2016). Innate sensing of oxidation-
512 specific epitopes in health and disease. Nat. Rev. Immunol. *16*, 485–497.

513 46. Rui, H., Yu, H., Chi, K., Han, Z., Zhu, W., Zhang, J., Guo, H., Zou, W., Wang, F., Xu, P., et
514 al. (2024). ALDH2 deficiency augments atherosclerosis through the USP14-cGAS-
515 dependent polarization of proinflammatory macrophages. Redox Biol. *76*, 103318.

516 47. Jones, C.L., Napier, B.A., Sampson, T.R., Llewellyn, A.C., Schroeder, M.R., and Weiss,
517 D.S. (2012). Subversion of host recognition and defense systems by Francisella spp.
518 Microbiol. Mol. Biol. Rev. *76*, 383–404.

519 48. Hamblin, K.A., Flick-Smith, H., Barnes, K.B., Pereira-Leal, J.B., Surkont, J., Hampson, R.,
520 Atkins, H.S., and Harding, S.V. (2019). Disulfiram, an alcohol dependence therapy, can
521 inhibit the in vitro growth of Francisella tularensis. Int. J. Antimicrob. Agents *54*, 85–88.

522 49. Quadros, R.M., Miura, H., Harms, D.W., Akatsuka, H., Sato, T., Aida, T., Redder, R.,
523 Richardson, G.P., Inagaki, Y., Sakai, D., et al. (2017). Easi-CRISPR: a robust method for

524 one-step generation of mice carrying conditional and insertion alleles using long ssDNA
525 donors and CRISPR ribonucleoproteins. Genome Biol. *18*, 92.

526 50. Brewer, T.F., Burgos-Barragan, G., Wit, N., Patel, K.J., and Chang, C.J. (2017). A 2-aza-
527 Cope reactivity-based platform for ratiometric fluorescence imaging of formaldehyde in
528 living cells. Chem. Sci. *8*, 4073–4081.

529 51. Ohata, J., Bruemmer, K.J., and Chang, C.J. (2019). Activity-Based Sensing Methods for
530 Monitoring the Reactive Carbon Species Carbon Monoxide and Formaldehyde in Living
531 Systems. Acc. Chem. Res. *52*, 2841–2848.

532 52. Ravesloot-Chavez, M.M., Van Dis, E., Fox, D., Nguyenla, X.H., Rawal, S.L., Ballinger,
533 M.A., Thomas, H., Kotov, D.I., Vance, R., Nachman, M., et al. (2023). Tuberculosis
534 susceptibility in genetically diverse mice reveals functional diversity of neutrophils. bioRxiv,
535 2023.06.29.547125. https://doi.org/10.1101/2023.06.29.547125.

536 53. Petersen, K.R., Streett, D.A., Gerritsen, A.T., Hunter, S.S., and Settles, M.L. (2015). Super
537 deduper, fast PCR duplicate detection in fastq files. In Proceedings of the 6th ACM
538 Conference on Bioinformatics, Computational Biology and Health Informatics BCB '15.
539 (Association for Computing Machinery), pp. 491–492.

540 54. Frankish, A., Diekhans, M., Ferreira, A.-M., Johnson, R., Jungreis, I., Loveland, J., Mudge,
541 J.M., Sisu, C., Wright, J., Armstrong, J., et al. (2019). GENCODE reference annotation for
542 the human and mouse genomes. Nucleic Acids Res. *47*, D766–D773.

543 55. Dobin, A., Davis, C.A., Schlesinger, F., Drenkow, J., Zaleski, C., Jha, S., Batut, P.,
544 Chaisson, M., and Gingeras, T.R. (2013). STAR: ultrafast universal RNA-seq aligner.
545 Bioinformatics *29*, 15–21.

546 56. Chang, X., Li, Z., Khac Thai, P.V., Minh Ha, D.T., Thuong Thuong, N.T., Wee, D., Binte
547 Mohamed Subhan, A.S., Silcocks, M., Eng Chee, C.B., Quynh Nhu, N.T., et al. (2025).
548 Genome-wide association study reveals a novel tuberculosis susceptibility locus in multiple
549 East Asian and European populations. medRxiv.
550 https://doi.org/10.1101/2024.03.14.24304327.

551 57. Shah, J.A., Warr, A.J., Graustein, A.D., Saha, A., Dunstan, S.J., Thuong, N.T.T., Thwaites,
552 G.E., Caws, M., Thai, P.V.K., Bang, N.D., et al. (2022). REL and BHLHE40 Variants Are
553 Associated with IL-12 and IL-10 Responses and Tuberculosis Risk. J. Immunol. *208*, 1352–
554 1361.

555 58. Khor, C.C., Do, T., Jia, H., Nakano, M., George, R., Abu-Amero, K., Duvesh, R., Chen, L.J.,
556 Li, Z., Nongpiur, M.E., et al. (2016). Genome-wide association study identifies five new
557 susceptibility loci for primary angle closure glaucoma. Nat. Genet. *48*, 556–562.

558 59. Dunstan, S.J., Hue, N.T., Han, B., Li, Z., Tram, T.T.B., Sim, K.S., Parry, C.M., Chinh, N.T.,
559 Vinh, H., Lan, N.P.H., et al. (2014). Variation at HLA-DRB1 is associated with resistance to
560 enteric fever. Nat. Genet. *46*, 1333–1336.

561 60. Hankin, J.H., Stram, D.O., Arakawa, K., Park, S., Low, S.H., Lee, H.P., and Yu, M.C.
562 (2001). Singapore Chinese Health Study: development, validation, and calibration of the
563 quantitative food frequency questionnaire. Nutr. Cancer *39*, 187–195.

61. Dorajoo, R., Chang, X., Gurung, R.L., Li, Z., Wang, L., Wang, R., Beckman, K.B., Adams-Haduch, J., M, Y., Liu, S., et al. (2019). Loci for human leukocyte telomere length in the Singaporean Chinese population and trans-ethnic genetic studies. Nat. Commun. *10*, 2491.

62. Chang, X., Gurung, R.L., Wang, L., Jin, A., Li, Z., Wang, R., Beckman, K.B., Adams-Haduch, J., Meah, W.Y., Sim, K.S., et al. (2021). Low frequency variants associated with leukocyte telomere length in the Singapore Chinese population. Commun Biol *4*, 519.

Acknowledgements: We thank Angus Y. Lee and Harmandeep S. Dhaliwal (UC Berkeley Cancer Research Laboratory) for generation of *Aldh2* mutant mice. We thank all the participants involved in the genetics studies in Vietnam. and Singapore. We acknowledge the clinical and laboratory staff at the study sites in Vietnam and Singapore for their contribution, especially Phan Vuong Khac Thai, Maxine Caws, Nguyen Duc Bang, Tran Thi Hong Chau, Guy Thwaites, and their teams at Oxford University Clinical Research Unit, and Pham Ngoc Thach Hospital for TB and Lung Diseases, Ho Chi Minh City, Vietnam. We thank Zheng Li from the Genome Institute of Singapore for his contribute to the TB GWAS. We thank Karen Elkins (FDA) for the gift of the Francisella LVS strain as well as helpful advice and protocols. **Funding:** We thank the NIH for the following support: ES 28096 (C.J.C.), AI066302 (R.E.V., S.A.S.), AI153197 (S.A.S., K.H.D.). C.J.C. is a CIFAR Fellow. R.E.V. is an Investigator of the Howard Hughes Medical Institute. The Vietnam human genetics work was supported by the National Health and Medical Research Council Australia: 1056689 (SJD) and 1172853 (SJD). The Singapore Chinese Health Study was supported by grants from the National Medical Research Council, Singapore (NMRC/CIRG/1456/2016), National Institutes of Health (R01 CA144034 and UM1 CA182876) and the Singapore Strategic Cohorts Consortium Award (23-1034-A0001). We thank the Office of Science & Research High-Containment Laboratories at NYU Grossman School of Medicine for their support in the completion of this research.

Author contributions: Conceptualization: KHD, SAS; Data Curation: SAS, KHD, SE, SB; Formal analysis: SE, SB, AB, XC, DK, DF, SAS; Investigation: SE, SB, AB, RB, DF, LT, AAS, LT; Resources: NTTT, RD, CCK, CKH, JMY, WPK, CJC, LT; Supervision: RV, SJD, SAS, KHD, CJC; Writing: SAS, SE, SJD; Review and Editing: all authors.

Competing interests: S.A.S. is on the SAB for X-biotix Therapeutics. R.E.V. is on the SAB for Tempest Therapeutics and X-biotix Therapeutics.

List of Supplementary Materials

Materials and Methods

Figures. S1-S4

601 **Materials and Methods**

602 *Ethics Statement*:

603 All procedures involving the use of mice were approved by the University of California (UC)
604 Berkeley, Institutional Animal Care and Use Committee (Protocol #2015-09-7979-1). All
605 protocols conform to federal regulations, the National Research Council Guide for the Care and
606 Use of Laboratory Animals, and the Public Health Service Policy on Humane Care and Use of
607 Laboratory Animals. All experiments handling *M. tuberculosis* were conducted in Biosafety Level
608 3 facilities in accordance with Environmental Health and Safety guidelines, and all experiments
609 handling *F. tularensis* LVS were conducted in Biosafety Level 2 facilities. Study protocols for
610 PTB human studies were approved by the Institutional Review Boards of Pham Ngoc Thach
611 Hospital for TB and Lung Disease and The Hospital for Tropical Diseases Ho Chi Minh City
612 (HCMC), Vietnam, HCMC Health Services, Vietnam and the Oxford Tropical Research Ethics
613 Committee, UK. Approval for the genetics study was also granted from the Health Sciences
614 Human Ethics Sub-Committee at the University of Melbourne, Australia (ID: 1340458). Written
615 informed consent was obtained from all participants. All studies in SCHS were approved by the
616 Institutional Review Board at National University of Singapore, and written informed consent
617 was obtained from all participants.

618

619 *Mice:*

620 C57BL/6J (#000664), *Nos2*$^{-/-}$, and p*47phox*$^{-/-}$ mice were obtained from The Jackson Laboratory
621 (Bar Harbor, ME) and bred in-house. *Sp140*$^{-/-}$ mice were generated previously[32] and bred in-
622 house. *Aldh2*$^{-/-}$ mice were generated in the process of recapitulating the human *ALDH2*2*
623 mutation in *Sp140*$^{-/-}$ mice. *Aldh2*2Sp140*$^{-/-}$ mice were generated by pronuclear injection of
624 Cas9 mRNA, sgRNA, and a 154 nucleotide ultramer oligo (IDT Inc., Coralville, IA) containing 77
625 and 39 nucleotide homology arms and encoding the *Aldh2*2* mutation as well as synonymous
626 mutations that disrupt sgRNA binding, as previously described[49]. Founder mice were genotyped
627 for *Aldh2*2* mutations by PCR using the forward primer 5' GGAGAGGTGTGCTGTGTT 3' and
628 the reverse primer 5' GGGATCTGTATTCCGTGGC 3' and then sequencing using the same
629 forward primer. Founders carrying the *Aldh2*2* mutation or deletions in *Aldh2* (i.e., *Aldh2*$^{-/-}$)
630 were bred one generation to *Sp140*$^{-/-}$, *Nos2*$^{-/-}$, or p47*phox*$^{-/-}$ mice to separate modified *Aldh2*
631 haplotypes. Resulting pups with matched *Aldh2* haplotypes were interbred to generate
632 homozygous lines that were maintained in-house.

633

634 *Bacterial Culture*:

635 Frozen stocks of low passage *M. tuberculosis* H37Rv, *M. tuberculosis* Erdman, and *M.*
636 *tuberculosis* Lux-Erdman (a reporter strain that constitutively expresses the bacterial luciferase
637 encoding luxCDABE operon, gift from Cox Laboratory at UC Berkeley) were grown to
638 logarithmic phase over 4-5 days at 37°C in Middlebrook 7H9 media with 10% albumin-dextrose-
639 saline, 0.5% glycerol, and 0.05% Tween-80 ("7H9c"). For preparation of aerosol stocks of *M.*
640 *tuberculosis* H37Rv and Erdman, logarithmic phase cultures were centrifuged at 3,500 rpm for 5
641 min., resuspended in 1X phosphate-buffered saline (PBS), and sonicated thrice for 30 sec. each
642 at 90% power. Cultures were then centrifuged at 700 rpm for 5 min to pellet large clumps, the
643 supernatant was collected, and then centrifuged again at 700 rpm for 5 min. The supernatant
644 was then collected and the optical density at 600 nM (OD_{600}) was measured to determine

645 bacterial concentration, and then aliquoted and frozen at -80°C until use. Frozen stocks of
646 FtLVS (generously gifted by Dr. Karen Elkins, FDA) were cultured in Mueller Hinton Broth
647 containing 1.25 mM $CaCl_2$, 2.2 mM $MgCl_2$, 0.1% glucose, 0.025% ferric pyrophosphate, and 2%
648 Isovitalex (#211875, Becton Dickinson, Franklin Lakes, NJ) to early log phase (OD600 ≈ 0.25)
649 overnight for use in experiments. For preparation of injection stocks of *F. tularensis* LVS, frozen
650 stocks were thawed at room temperature and then diluted in sterile 1X PBS to the desired
651 concentration.
652
653 We used a standardized IC_{50} assay. Briefly, bacteria were grown to an OD_{580} ~0.5-1, collected
654 by centrifugation, and resuspended in acidified 7H9c. Bacteria were then diluted to an OD580 of
655 0.02 and 198 µl aliquoted into 30 wells per test condition in 96-well plates. Two-fold dilutions of
656 aldehyde stocks were made and 2 µl of each added in triplicate wells. OD580 was measured in
657 a Molecular Devices M3 plate reader five days later. Data were plotted in GraphPad Prism Plot
658 the data in Prism.
659
660 *In Vitro Macrophage Isolation and Culture:*
661 Bone-marrow was obtained from *Aldh2*$^{-/-}$, *Aldh2*$^{-/-}$*Sp140*$^{-/-}$, *Sp140*$^{-/-}$, *Nos2*$^{-/-}$, *Nos2*$^{-/-}$*Aldh2*$^{-/-}$,
662 *p47phox*$^{-/-}$, p*47phox*$^{-/-}$*Aldh2*$^{-/-}$, and C57BL/6J mice and cultured in DMEM (#11960-044,
663 Thermo Fischer Scientific, Waltham, MA) containing 10% FBS, 2 mM L-glutamine, and 10%
664 supernatant from 3T3-M-CSF cells (BMDM media) for 6 days with media supplementation on
665 day 3 to generate bone marrow-derived macrophages (BMDMs). BMDMs were then harvested
666 and frozen in liquid nitrogen in 40% FBS, 10% DMSO, and 50% BMDM media until use.
667
668 *In Vitro Macrophage Infections:*
669 For infection with *M. tuberculosis*, BMDMs were plated in 96-well plates at $5x10^4$ cells/well and
670 allowed to adhere for 48 hours prior to infection. 24 hours prior to infection, media was changed
671 and BMDMs were stimulated with IFNγ (≈ 30 ng/mL) for IFNγ+ conditions. 5 days prior to
672 infection, a frozen stock of *M. tuberculosis* Lux-Erd was thawed and cultured in 7H9 at 37°C to
673 log phase (OD600 = 0.2 – 1.0). *M. tuberculosis* was centrifuged at 3500 rpm for 5 min. and
674 washed twice in PBS, centrifuged at 500 rpm for 5 min. to pellet clumps, and then sonicated at
675 90% power (twice, 30 sec. each). After sonication, cultures were diluted in DMEM + 5% horse
676 serum + 5% FBS and added to the BMDMs at a multiplicity of infection (MOI) of 1, followed by
677 spinfection at 1200 rpm for 10 min. Supernatant was then removed and the infected BMDMs
678 were washed twice with 1X PBS before the appropriate media was added, and the cells were
679 incubated at 37°C/5% CO_2 until the first time point. CFU were enumerated at the indicated time
680 points by washing infected cells twice with PBS, lysing in sterile-filtered deionized water with
681 0.5% Triton X-100 for 10 min. at 37°C/5% CO_2, and performing serial dilutions in 1X PBS
682 containing 0.05% Tween 80 before aliquoting dilutions onto Middlebrook 7H10 plates
683 supplemented with 0.5% glycerol and 10% OADC (Middlebrook) and incubated for 21 days at
684 37°C. CFU is normalized to inoculum dose, calculated by plating t = 0 CFU immediately after
685 spinfection. For infection with FtLVS, BMDMs were prepared as described above. BMDMs were
686 plated in 96-well plates at $5x10^4$ cells/well and allowed to adhere for 48 hours prior to infection.
687 24 hours prior to infection, media was changed and BMDMs were stimulated with IFNγ (≈ 30
688 ng/mL) for IFNγ positive conditions. To infect the BMDMs, FtLVS stocks were thawed,

689 resuspended in BMDM media, added to the BMDMs at an MOI = 1 and allowed to phagocytose
690 for 2 hours at 37°C/5% CO_2. After phagocytosis, infected BMDMs were washed thrice with 1X
691 PBS and then supplemented with normal media until predetermined time points. To enumerate
692 CFU/well, BMDMs were rinsed once with 1X PBS, lysed with sterile-filtered deionized water for
693 10 min., and then serial dilutions were plated on Mueller Hinton plates containing 85 mM NaCl,
694 1% (w/v) proteose peptone/tryptone, 8% (w/v) bacto-agar, 0.1% glucose, 0.025% ferric
695 pyrophosphate, 2% Isovitalex, and 2.5% bovine serum for 3 days at 37°C/5% CO_2 until CFU
696 were counted. Cell viability was determined using cell titer glow according to the manufacturer's
697 protocol. For 4HNE quantification in infected BMDMs, cells were treated as described above
698 and infected via centrifugation at 1200rpm for 10 minutes prior to the generation of cell lysate.
699
700 *Aldehyde Quantification:*
701 To measure formaldehyde, BMDMs were plated in 96-well plates at $5x10^4$ cells/well and allowed
702 to adhere for 48 hours prior to analysis. 24 hours prior to analysis, BMDMs were stimulated with
703 IFNγ (≈ 30 ng/mL) and PAM3CSK4 (50 ng/mL). BMDM formaldehyde levels were quantified
704 using Mito-RFAP-2, a mitochondrial-targeted version of ratiometric formaldehyde dye RFAP-2
705 [50,51]. Briefly, Mito-RFAP-2 was dissolved in DMSO to a concentration of 10 mM and diluted to 10
706 μM in Hank's Balanced Salt Solution (HBSS); the probe was then added to the BMDMs for 30
707 min. at 37°C/5% CO_2. BMDMs were then rinsed once with HBSS to remove the probe and
708 allowed to incubate in BMDM media for 60 min. at 37°C/5% CO_2. The cells were then analyzed
709 by fluorescent excitation at 405 nm and 488 nm and emission at 510 nm. Fluorescence was
710 measured using a SpectraMax M3 plate reader (Molecular Devices, San Jose, CA) and
711 reported as the ratiometric value of emission at 405 nm and 488 nm excitations.
712
713 BMDM 4HNE levels were quantified by ELISA (abcam, ab287803). Cells were plated at $5x10^5$
714 cells per/well in 24-well plates and allowed to adhere for 48 hours prior to analysis. 24 hours
715 prior to analysis, BMDMs were stimulated as described above or infected with FtLVS at an MOI
716 of 1. Two hours after infection, cells were washed 1x with warm PBS and then lifted using cold
717 PBS. Cells were then pelleted and lysed, and lysates were processed for 4HNE quantification
718 according to the manufacturer's protocol. To measure 4HNE in murine tissues, mice were
719 infected with 10^5 *FtLVS* i.d.. Organs were harvested at 3 dpi and processed for quantification by
720 ELISA according to the manufacturer's protocol (abcam, ab287803).
721
722 *Immunoblotting:*
723 BMDMs were prepared as previously described and plated in a 24-well plate at $3x10^5$ cells/well,
724 and infected with *M. tuberculosis* H37Rv according to the previously described protocol. 24
725 hours post infection, BMDMs were rinsed with 1X PBS and lysed with Laemmli Buffer
726 (#1610737EDU, Bio Rad, Hercules, CA). Samples were heat inactivated/sterilized at 100°C for
727 20 min. prior to removal from the BSL3 facility. Protein lysates were prepared by heating in 1X
728 SDS for 5 min. at 100°C and then analyzed by SDS-PAGE using 4-20% Criterion TGX Precast
729 Protein Gel (#5678094, Bio Rad), rabbit monoclonal antibody (EPR4494) against ALDH2
730 (#ab133306, Abcam, Cambridge, MA), and an anti-rabbit HRP-conjugated secondary antibody.
731 Blots were developed with Western Lightning Plus-ECL enhanced chemiluminescence

732 substrate (#NEL103001EA, PerkinElmer, Waltham, MA) and a ChemiDoc MP/475D Imaging
733 System (Bio Rad).
734
735 *Bulk and Single Cell RNAseq:*
736 Single cell RNA sequencing results were extracted from a previously published dataset[52] on *M.*
737 *tuberculosis*-infected B6 mice. For bulk RNAseq, BMDMs were prepared as previously
738 described and plated in a 24-well plate at $3x10^5$ cells/well, and infected with *M. tuberculosis*
739 H37Rv according to the previously described protocol. 24 hours post infection, BMDM media
740 was removed and cells were lysed with TRIzol Reagent (#15596018, Thermo Fisher Scientific).
741 RNA was extraction was performed by adding chloroform and centrifuging samples to make a
742 biphasic mixture containing RNA in an aqueous phase. The RNA-containing phase was then
743 collected and cleaned up using a RNeasy Mini Kit (#74104, Qiagen, Hilden, Germany) with on-
744 column DNase digestion according to the manufacturer's protocol. The isolated RNA was then
745 quantified and analyzed by a Qubit Quantitation Platform and an Agilent 2100 Bioanalyzer,
746 respectively, at the Functional Genomics Laboratory of the California Institute for Quantitative
747 Biosciences (UC Berkeley) and then submitted to GeneWiz/Azenta Life Sciences (South
748 Plainfield, NJ) for library preparation and sequencing. Each sample was dual indexed using
749 NEBNext multiplex oligomers and then quantity and quality were assessed with a Qubit Broad
750 Range Kit and bioanalyzer, respectively. All samples had a RIN > 9.8 and 100 ng of total RNA
751 was used in library preparation. Samples were then prepared for sequencing using a NEBNext
752 Ultra II RNA-seq with Poly-A selection kit and sequenced on a NovaSeq 6000 S4 (partial lane),
753 with a sequencing depth of 29 million paired-end reads per sample. Illumina sequencing data
754 files were pre-processed with HTStream (v. 1.3.0) to remove PCR duplicates, trim adapters,
755 polyA tails, and N characters, and to remove low quality 3' and 5' bases[53] and were checked for
756 quality with FastQC (v. 0.11.7). Sequences were aligned to the mouse primary assembly
757 GRCm39 from GENCODE[54] and gene counts were generated using STAR (v.
758 2.7.10b_alpha_230301[55]).
759
760 *Aldehyde susceptibility assays:*
761 *M. tuberculosis* H37Rv was cultured as described above. To test susceptibility to various
762 aldehydes, cultures were grown to an optical density at 580 nm (OD_{580}) of 0.8-1.0. Bacteria
763 were collected by centrifugation at 3,200 *g* and resuspended in 7H9c acidified to pH 5.5 with 1N
764 HCl and clumped cells were removed with a slow-speed spin at 150 *g*. The supernatant was
765 diluted to an OD_{580} of 0.08. 200 µl of bacteria was added to wells of a 96-well plate; for each
766 condition tested, three wells were prepared. Two µL of 1:100 aldehyde stock solutions were
767 added to each well to obtain the final concentrations indicated in the Figure 2 (A-C). Exposure
768 was carried out for a period of six days. Aldehydes were purchased from the following: 4-
769 hydroxynonenal (4HNE) (# 32100, Cayman Chemical, Ann Arbor, MI), malondialdehyde (MDA)
770 (#63287, Millipore Sigma, Burlington, MA), and formaldehyde (FA) (#15710, Electron
771 Microscopy Sciences, Hatfield, PA) (16% paraformaldehyde solution, stored in aliquots at -
772 20˚C). To generate nitric oxide (NO), sodium nitrite was added to a final concentration of 3 mM.
773 To test the susceptibility of *F. tularensis* LVS to various aldehydes, we followed a previously
774 described protocol[33]. Briefly, *F. tularensis* LVS was plated on Mueller Hinton plates for 3 days at
775 37°C/5% CO_2. Multiple colonies colony were then scraped and used to inoculate a liquid culture

776 (to ensure diversity of the culture) that was maintained at 37°C/180 rpm for 12-14 hours. The
777 culture was then washed twice in 1X PBS and resuspended at an OD600 = 0.01 in 1X PBS and
778 aliquoted into a 96-well plate containing various concentrations of 4HNE (#32100, Cayman
779 Chemical Company), or FA (#F1635, Millipore Sigma) and incubated for 2 hours at 37°C/5%
780 CO_2. After incubation, CFU/well was enumerated for each condition by plating serial dilutions of
781 the culture on Mueller Hinton plates and incubating at 37°C/5% CO_2 for 3 days.
782
783 *In Vivo Pathogen Challenge:*
784 Mice were infected with *M. tuberculosis* H37Rv (*Aldh2*$^{-/-}$ and B6 mice), or *M. tuberculosis*
785 Erdman (*Aldh2*$^{-/-}$ and *Aldh2*$^{-/-}$ *Sp140*$^{-/-}$ mice) *via* the aerosol route. Aerosol infection was
786 performed using a nebulizer and full-body inhalation exposure system (Glas-Col, Terre Haute,
787 IN). Previously prepared aerosol stocks were thawed and 9 mL of culture diluted into sterile-
788 filtered deionized water was loaded into the nebulizer calibrated to deliver ~25 CFU/mouse, as
789 measured by CFU in the lungs 1 day following infection (data not shown). At predetermined time
790 points, mice were euthanized, and the lungs were mechanically homogenized in 1X PBS
791 containing 0.05% Tween 80 and serial dilutions were plated on 7H10 plates and incubated for
792 21 days at 37°C until CFU were counted. For mice infected with *F. tularensis* LVS, injection
793 stocks were prepared as previously described and ~10^5 CFU were administered intradermally,
794 as measured by plating serial dilutions of the inoculum on Mueller Hinton plates (data not
795 shown). Due to the immunocompromised nature of *Nos2*$^{-/-}$ and *Phox-p47*$^{-/-}$ mice, experiments
796 involving these genotypes used an inoculum of ~10^3 CFU. 3 or 5 dpi, mice were euthanized,
797 and their lungs and spleens were mechanically homogenized in 1X PBS. Serial dilutions were
798 plated on Mueller Hinton plates and incubated for 3 days at 37°C/5% CO_2 until CFU were
799 counted. For survival studies, mice were infected, monitored daily for weight loss, and
800 euthanized when weight loss exceeded 15% baseline body weight.
801
802 *Tissue Processing for Flow Cytometry:*
803 Mice were harvested at 3 dpi for flow cytometry analysis and quantification of bacterial burden
804 (CFU). To create single cell suspensions of organs for analysis, lungs were collected into
805 gentleMACS C tubes (Miltenyi Biotec) containing 3 mL of complete RPMI (cRPMI)
806 supplemented with 70 µg/mL Liberase TM (Merck) and 30 µg/mL DNase I (Millipore Sigma).
807 Tissues were mechanically dissociated using the gentleMACS disassociator (lung_01 program)
808 followed by enzymatic digestion for 30 minutes at 37 °C. Samples were then homogenized into
809 single-cell suspensions using the lung_02 gentleMACS program. Digestion was quenched with
810 2 mL PBS containing 20% fetal bovine serum (Thermo Fisher Scientific), and suspensions were
811 passed through 70 µm cell strainers. Spleens were homogenized by manual dissociation
812 through 70 µm cell strainers.
813
814 *Flow Cytometry:*
815 For flow cytometry, spleen and lung single-cell suspensions were pelleted and resuspended in
816 2 mL PBS. A 200 µL aliquot was blocked with BD α-mouse CD16/32 Fc block for 30 minutes at
817 room temperature. Cells were then surface stained for 30 hour at room temperature with
818 optimized dilutions of the following antibodies: BUV805-labeled CD45 (BD 752415), BUV563-
819 labeled Ly6C (BD 755198), BUV496-labeled CD11c (BD 750450), BV786-labeled CD64 (BD

569507), BV605-labeled CD11b (BioLegend 101257), PerCP-Fire806-labeled Siglec-F (BioLegend 155536), FITC-labeled MerTK (BioLegend 151504), PE-Cy7-labeled NK1.1 (BioLegend 108714), APC-Cy7-labeled Ly6G (BioLegend 127623). Cells were then buffer exchanged to PBS then stained with Aqua LIVE/DEAD fixable viability dye (Invitrogen L34957) fo 30 minutes at room temnperature. Stained samples were fixed for 20 minutes at room temperature using Cytofix/Cytoperm (BD Biosciences). For intracellular staining, fixed cells were incubated with PE-labeled iNOS (BioLegend 696806) and APC-labeled Arg-1 (Invitrogen 17-3697-82). To determine absolute cell counts, fluorescent CountBright counting beads (Invitrogen) were added to each sample. Data were acquired on a Symphony A3 flow cytometer (BD Biosciences) and analyzed using FlowJo version 10 (BD Biosciences).

Cytokine quantification:

Mice were infected with 10^5 FtLVS I.d.. Tissues were harvested at 3 dpi and homogenized using a Cole-Parmer Tissue-Homogenizer (UX-04727-01). Cytokine concentrations in tissue homogenates were quantified using a LEGENDplex™ Mouse Inflammation Panel (Biolegend) per manufacturer's protocol with volumes adjusted for a 384 well plate format.

Candidate Gene Analysis Study:

Study subjects from the Vietnam human genetics collection and the SCHS have been described in detail previously[56]. In brief, the Vietnamese PTB participants were recruited at district TB units in Ho Chi Minh City, Vietnam as part of larger clinical studies with strictly defined clinical phenotypes[57]. Patients sampled for the genetics study were 18 years or older, HIV negative, had no previous history of TB treatment and were sputum smear positive. The Vietnamese population controls are otherwise healthy adults with primary angle closure glaucoma who have been previously described[58]. DNA from all participants were genome wide genotyped on either the Infinium OmniExpress-24 or OmniExpress-12 array and standard quality control measures and pipelines were applied as described previously[58,59] (PMID: 40313261). SCHS is a long-term prospective population-based cohort study focused on genetic and environmental determinants of cancer and other diseases in Singapore[60]. From April 1993 to December 1998, the study recruited 63,257 participants of Singaporean Chinese descent, hailing from the Hokkien and Cantonese dialect groups. Starting from April 1994, a random subset of 3% of participants were invited to contribute blood/buccal cell and spot urine samples. In January 2001, the collection of biospecimens was expanded to include all enrolled participants who provided consent and approximately half of all study participants donate blood or buccal samples for genetic studies. PTB cases were identified through linkage with the National Tuberculosis Notification Registry. Diagnosis is primarily based on passive case detection, where individuals seek medical attention for symptoms such as persistent cough, blood-stained sputum, fever, chills, and night sweats. Confirmatory diagnosis involved a positive sputum smear and microbiological culture of *M. tuberculosis*. Most notifications are reported by public hospitals and the Tuberculosis Control Unit and are supplemented by electronic records from the two mycobacterial laboratories in Singapore, ensuring thorough case capture in the national registry. A total of 27,308 samples were whole genome genotyped using the Illumina Global Screening Array (GSA). An additional 2,161 independent subjects from the SCHS CAD-nested case-control study were genotyped on

863 Illumina HumanOmniZhonghua Bead Chip. Comprehensive information regarding genotyping
864 and QC protocols has been previously published[61,62].
865
866 Genotype data for rs671 was extracted from genotyping array data for subsequent statistical
867 analysis. Logistic regression was applied with adjustment for the first three principal
868 components (PCs) to control for any potential population structure. The analysis was conducted
869 separately for the Vietnamese and the SCHS followed by meta-analysis using a fixed-effect
870 inverse-variance weighted (IVW) method. Cochran's Q ($P_{Het} < 0.05$) were evaluated as an
871 indication of heterogeneity. All analysis was conducted using Stata/SE15.1(Statacorp, College
872 Station, TX, USA).
873
874 *Statistical Analysis:*
875 Data are presented as mean values and error bars represent standard deviation. The number of
876 samples, experimental replicates, and statistical tests are described in the legend of each figure.
877 Statistical analyses were performed using GraphPad Prism 9 (GraphPad, La Jolla, CA) and a p
878 < 0.05 was considered significant.
879
880
881
882
883

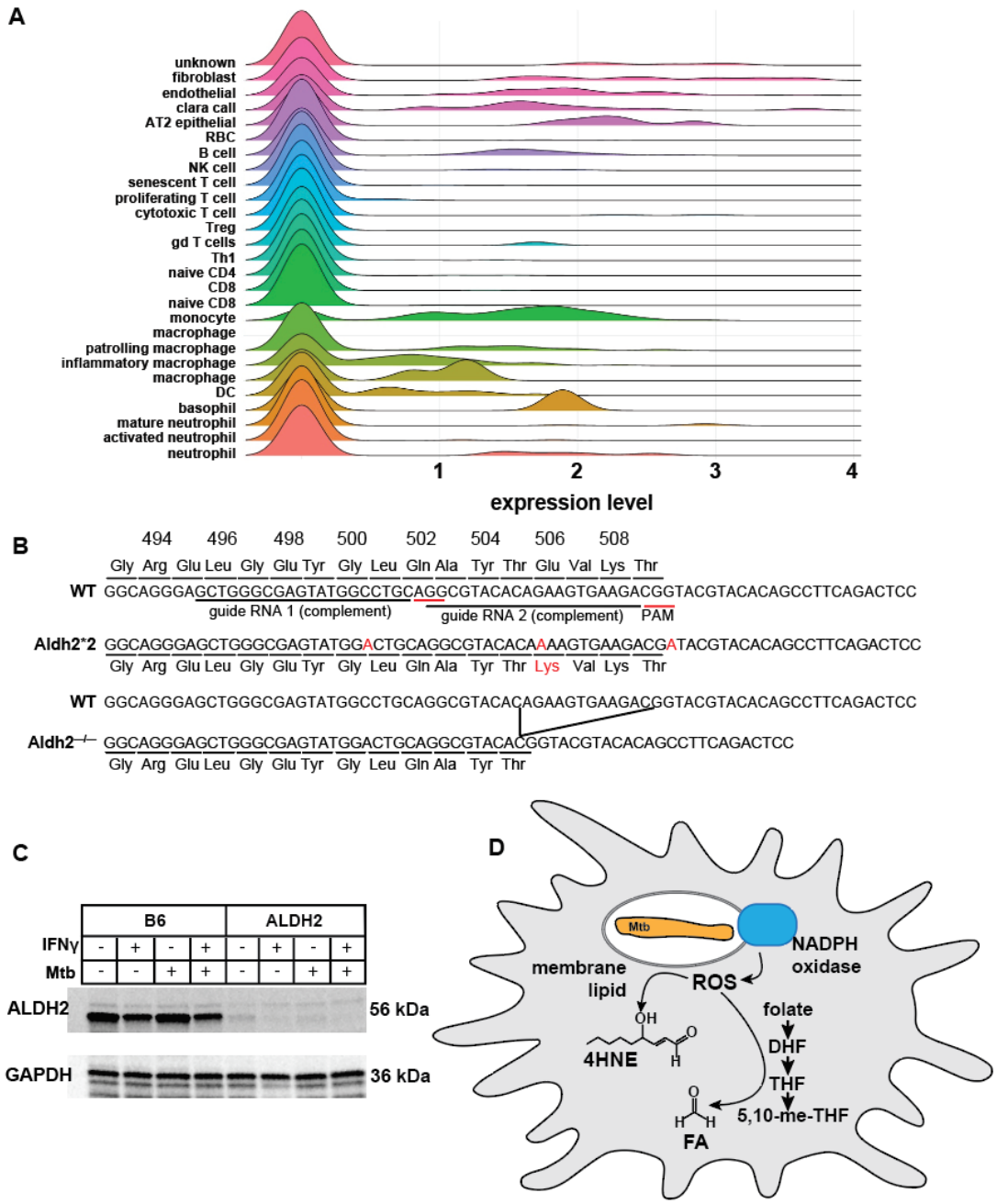

Figure S1. Genetic knock out of *Aldh2* inhibits ALDH2 production

(A) Expression of *Aldh2* in indicated cell types in C57BL/6 mice infected with Mtb for 3 weeks. (B) CRISPR targeting strategy of *Aldh2*2* mice, resulting in mutants containing three adenine point mutations (first and third adenines disrupt sgRNA binding, while second adenine is the human mutation) (*Aldh2*2* mice) and mice containing a 12 bp (four amino acid) in-frame deletion (*Aldh2*$^{-/-}$ mice). (C) Immunoblot of WT and *Aldh2*$^{-/-}$ BMDM cell lysates stained with αALDH2 (56 kDa) and αGAPDH (36 kDa, control). (D) Model of macrophage sources of 4HNE and FA. 4HNE is derived from peroxidation of host lipids induced in part by activity of reactive oxygen species (ROS) produced by NADPH oxidase acting on cell membranes. Formaldehyde

894 (FA) is derived from decomposition of tetrahydrofolate and its derivatives in a process that is
895 accelerated by ROS.
896
897

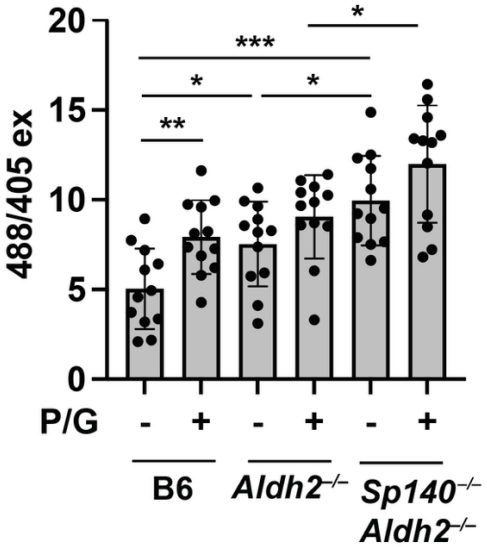

898
899
900 **Figure S2. *Sp140*$^{-/-}$*Aldh2*$^{-/-}$ demonstrate increased mitochondrial aldehyde levels**
901 **(**A) WT, *Aldh2*$^{-/-}$, and *Sp140*$^{-/-}$*Aldh2*$^{-/-}$ BMDM mitochondrial-associated formaldehyde levels
902 after 24 hours stimulation with IFNγ and TLR2-agonist PAM3CSK4 *in vitro* (n = 3 independent
903 experiments, B6 and *Aldh2*$^{-/-}$ results are same as reported in Figure 3A). *, $p < 0.05$, **, $p <$
904 0.01, ***, $p < 0.001$, Unpaired t-test.
905
906

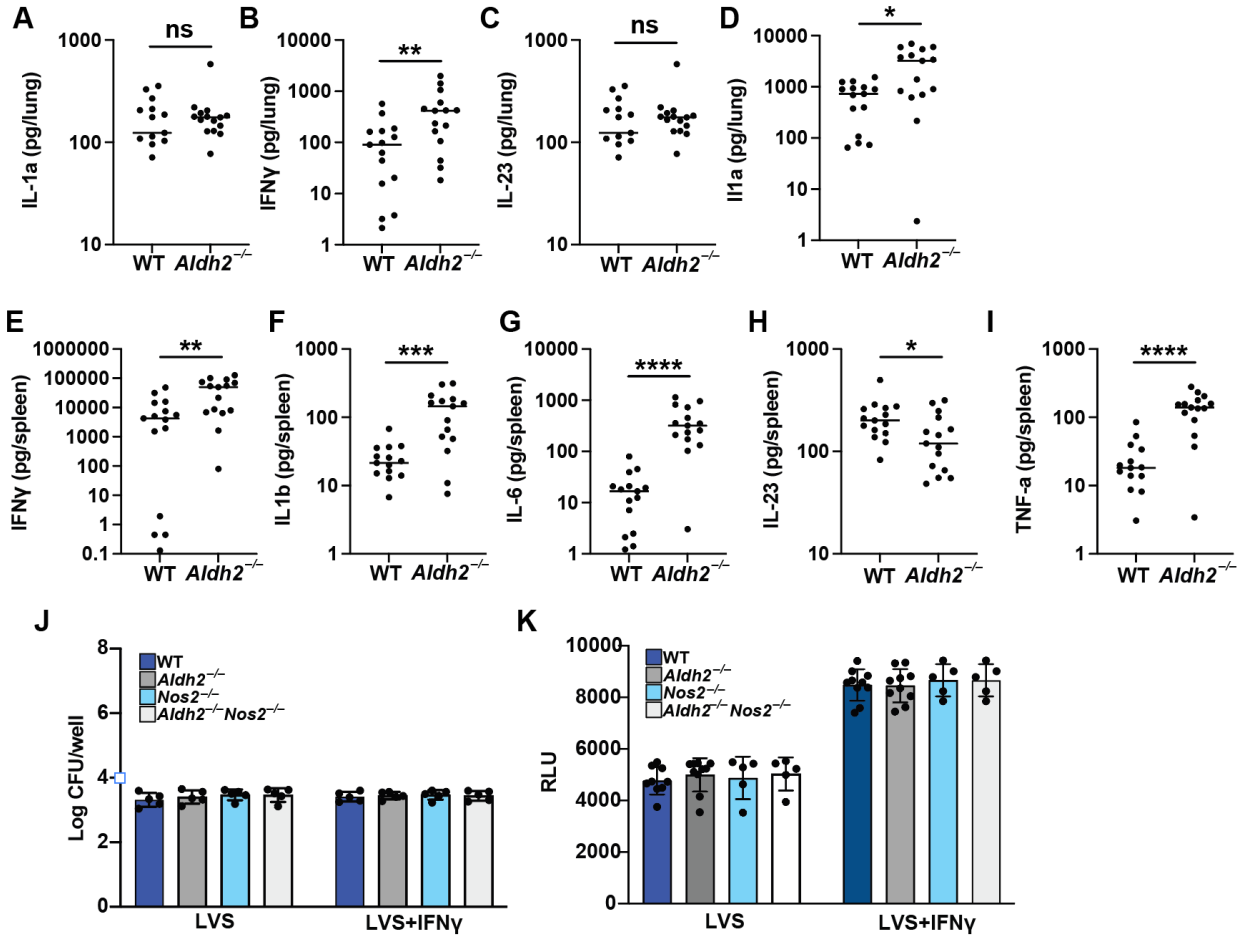

907

908

Figure S3. *Aldh2* deficiency confers iNOS-independent resistance to FtLVS with altered lung and spleen cytokines

Quantification of Il-1a (A), IFNγ (B), IL-23 (C), and IL1a (D) in the lungs of WTand *Aldh2*$^{-/-}$ mice infected with 10^5 FtLVS i.d., 3 dpi. Quantification of IFNγ (E), IL1b F), Il-6 (G), IL-23 (H), TNF-a (I) in the spleens of WT and *Aldh2*$^{-/-}$ mice infected with 10^5 FtLVS i.d., 3 dpi. (J) CFU enumeration in WT, *Aldh2*$^{-/-}$, *Nos2*$^{-/-}$, and *Nos2*$^{-/-}$*Aldh2*$^{-/-}$ infected with FtLVS MOI=1, +/- IFNγ 0 hours post infection. (K) Viability of B6, *Aldh2*$^{-/-}$, *Nos2*$^{-/-}$, and *Nos2*$^{-/-}$*Aldh2*$^{-/-}$ BMDMs infected with FtLVS MOI=, 1 +/- IFNγ , 2 dpi. (A-I): unpaired t-test. (J-K): 2way ANOVA with Tukey's multiple comparisons test. Data in (J-K) correspond with results in figure 3G. *p<0.05, **p<0.01, ***p<0.001, ****p<0.0001. Experiments are representative of a minimum of three (J), (K) or three experiments combined (A-I).

909

910

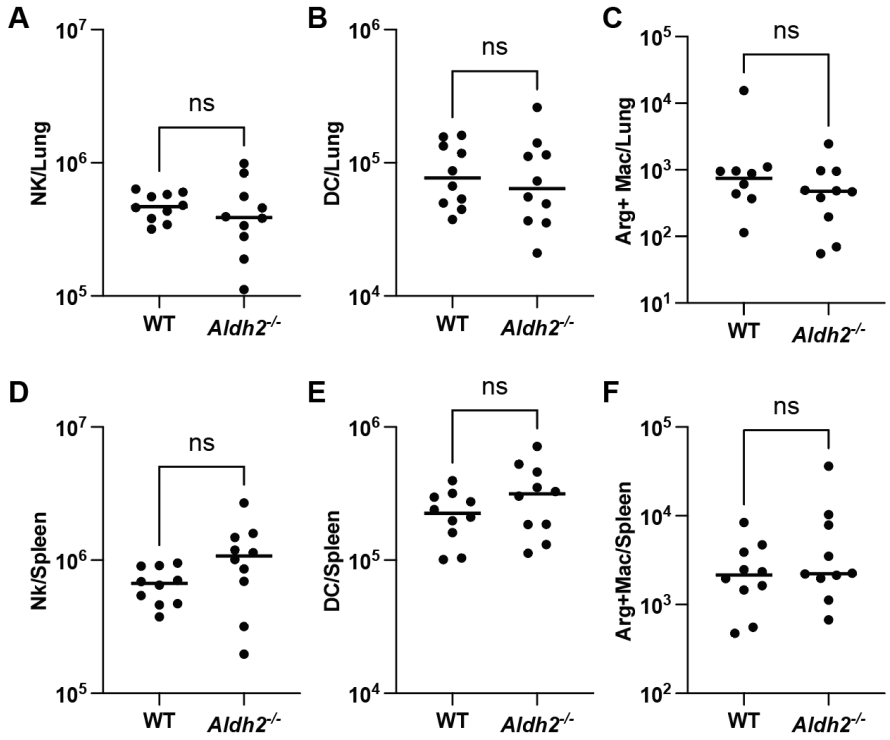

911

912

913 **Figure S4. Immune cell frequencies in organs of FtLVS infected, *Aldh2*$^{-/-}$ and WT mice**
914 Frequencies of natural killer (NK) cells (A) dendritic cells (B) arginase-positive (Arg+)
915 macrophages (C) in the lungs of WT and *Aldh2*$^{-/-}$ mice infected with 10^5 FtLVS i.d., 3 dpi.
916 Frequencies of natural killer (NK) cells (D) dendritic cells (E) arginase-positive (Arg+)
917 macrophages (F) in the spleens of WT and *Aldh2*$^{-/-}$ mice infected with 10^5 FtLVS i.d., 3 dpi.
918 (A-J) correspond with results in figure 4A-J. *p<0.05, **p<0.01, ***p<0.001, ****p<0.0001
919 (A-D): unpaired t-test. (E-F): Mann-Whitney test. Experiments are representative of a
920 minimum of three experiments.